Chinese Journal of Aeronautics, 2013,26(3): 606–613

Chinese Society of Aeronautics and Astronautics
& Beihang University

Chinese Journal of Aeronautics

cja@buaa.edu.cn
www.sciencedirect.com

Study on ballistic penetration resistance of titanium alloy TC4, Part II: Numerical analysis

Zhang Tao [a], Chen Wei [a,*], Guan Yupu [a], Gao Deping [a], Li Shuguang [b]

[a] *College of Energy and Power Engineering, Nanjing University of Aeronautics and Astronautics, Nanjing 210016, China*
[b] *Engineering Department, CITIC Offshore Helicopter Co., Ltd., Shenzhen 518052, China*

Received 21 December 2011; revised 10 April 2012; accepted 24 May 2012
Available online 28 April 2013

KEYWORDS

Absorbed energy;
Casing;
Containment;
Critical velocity;
Failure mechanism;
Simulation

Abstract Enhancing containment capability and reducing weight are always great concerns in the design of casings. Ballistic tests can help to mitigate a catastrophic event after a blade out, yet taking time and costing money. A wise way is to hunt for a validated numerical simulation technology, through which the material dynamic behavior over the strain rate range in the ballistic tests should be represented and reasonable failure strain should be defined. The simulation results show that the validation of the numerical simulation technology based on the test data can accurately estimate the absorption energy, describe the physical process and failure mode during the penetration, as well as the failure mechanism. It is found that energy dissipation of projectiles is in manner of compression stage, energy conversion stage, and interactive scrap stage. An effect indicator is proposed, where the factors of critical velocity including impact orientation and mass of projectiles and thickness of casings are considered. The critical velocity presents a linear relation with the effect indicator, which implies the critical velocity obtained by the flat casing could underestimate the capability of the real casing.

1. Introduction

The ballistic impact tests of flat and subscale casings of TC4 were presented in Ref.[1] However, due to the complexity of impact problems, it is not an optimum scheme to base all research on ballistic tests alone. Therefore, a high-precision numerical method is requested as an alternative technique to supplement the limited tests. In this paper, the explicit finite element code LS-DYNA is used to provide insight into the ballistic penetration resistance of TC4.

Nowadays, the finite element codes are capable of settling problems as complex as perforation processes and modeling simulation on dynamic characteristics accurately. A great deal of numerical simulation work has been proposed in the open literature, for example, Shmotin et al.,[2] and Sinha et al.[3] use LS-DYNA to simulate the fan blade out events. Though commercial finite element software has reached a state of maturity, the main challenge of the explicit finite element is associated with reliable material descriptions.[4] Earlier studies by Jonas and Zukas[5] have indicated that errors associated with material properties are usually far greater than those inherent in the numerical method.

* Corresponding author. Tel.: +86 25 84890515.
E-mail addresses: ericzh1210@yahoo.com.cn (T. Zhang), chenwei@nuaa.edu.cn (W. Chen), ypguan@nuaa.edu.cn (Y. Guan), gdp202@nuaa.edu.cn (D. Gao), lisg@china-cohc.com (S. Li).

Peer review under responsibility of Editorial Committe of CJA.

1000-9361 © 2013 Production and hosting by Elsevier Ltd. on behalf of CSAA & BUAA. Open access under CC BY-NC-ND license.
http://dx.doi.org/10.1016/j.cja.2013.04.013

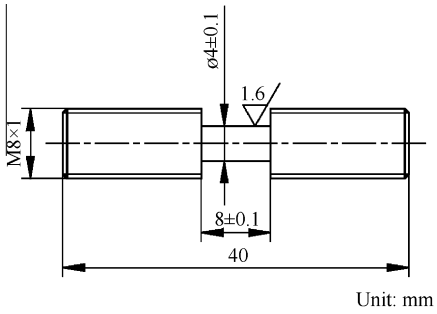

Fig. 1 The specimen of dynamic tensile.

When subjected to moderate velocity impact, the dynamic mechanical properties of titanium alloy are more significantly different from those in static state. Zhao and Li[6] conducted an experiment through Split Hopkinson Tension Bar (SHTB) Program on titanium alloy TC4, with its strain rates ranging from 68 s^{-1} to 502 s^{-1}, and the test results indicate that TC4 is sensitive to strain rate and the dynamic yield stress and flow stress increase obviously compared with the static ones. Thus, to be able to predict various phenomena taking place during ballistic perforation, a strain rate dependent dynamic constitutive model should be used.

The plastic kinematic hardening (P-K) material model turns out to be effective for modeling dynamic properties and accurately representing a wide range of strain rates of materials during moderate velocity impact. It is very suited to model material properties, with a combination of kinematic and isotropic hardening and the maximum strain failure criterion being used. The Bauschinger effect of metals is also modeled in the model. Moreover, according to Boyer et al.,[7] TC4 is susceptible to the Bauschinger effect, especially at room temperature. The P-K model has been proved numerically robust and can be easily used in simulating impact.[8,9]

In this paper, the P-K constitutive model is chosen to represent the deformation and failure response of TC4 subjected to impact. The material constants of the P-K are identified from different strain rate tests by the SHTB technique and the failure criterion of the model is calibrated by the proposed flat and subscale casings' ballistic test results. The penetration resistance of the two scales of casings is evaluated by predicting the impact responses of the penetration data from both the test and numerical simulation.

2. Analysis model

2.1. Constitutive model

The P-K model is a strain rate dependent elastic plastic material model. In this model, strain rate is reflected in the Cowper-Symonds model which is used almost exclusively in theoretical and numerical studies on dynamic plastic behaviors of strain rate sensitive materials.[10] The Cowper-Symonds model scales the yield stress σ_y by the strain rate dependent factor as shown below[11]:

$$\sigma_y = \left[1 + (\dot{\varepsilon}/C)^{1/p}\right]\left(\sigma_0 + \beta E_p \varepsilon_p^{eff}\right) \quad (1)$$

where C and p are the Cowper-Symonds strain rate parameters, σ_0 is the initial yield stress, $\dot{\varepsilon}$ the strain rate, ε_p^{eff} the effective plastic strain, and E_p the plastic hardening modulus, β the hardening parameter between 0 and 1. The effect of kinematic and isotropic hardening degree on the material yield surface can be chosen by adjusting β.

The influence of strain rate on dynamic yield stress and plastic hardening process on dynamic flow stress are uncoupled from each other in Eq. (1), and the model is purely empirical. The maximum strain failure criterion is described in the model. Fracture is simulated by removing elements when the strain reaches the defined failure strain ε_f.

2.2. Material property test

To determine the model constants and obtain meaningful numerical results, it is necessary to study dynamic behaviors of materials at high strain rate in the projectile impact. The target material property test of TC4 is implemented by different strain rate tests. These high strain rate tests are done by using the SHTB technique and data is obtained at the strain rates of 10^{-3}–4×10^3 s^{-1}. The specimen of dynamic tensile is shown in Fig. 1. In order to calibrate the gauge of the test material and provide data to support high strain rate tests, a quasi tensile test should be performed by the material testing machine. The geometry of the specimen for the quasi-static tensile test is presented in Fig. 2.

The typical tensile specimens after SHTB tests are shown in Fig. 3. For the strain rate of 500 s^{-1}, the specimen exhibits very uniform deformation with no indication of necking. However, for the strain rate of 1000 s^{-1}, the specimen decreases in the cross-sectional area. For the strain rate of 2000 s^{-1}, the typical ductile fracture feature is shown. Ductile fracture surfaces have large necking regions with an overall rough and irregular appearance. For the strain rate of 4000 s^{-1}, the specimen is

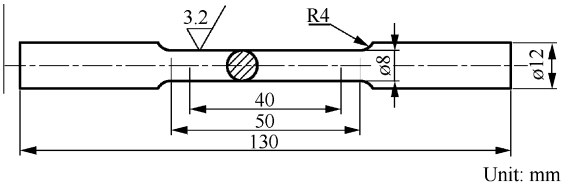

Fig. 2 The specimen of the quasi-static tensile test.

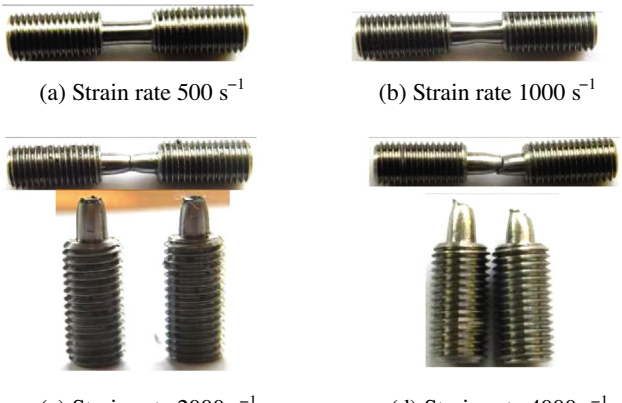

(a) Strain rate 500 s^{-1} (b) Strain rate 1000 s^{-1}

(c) Strain rate 2000 s^{-1} (d) Strain rate 4000 s^{-1}

Fig. 3 The specimens after tensile tested.

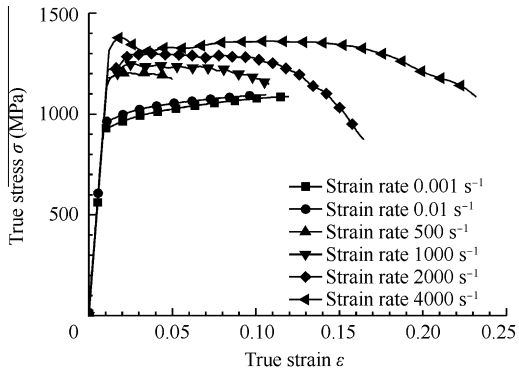

Fig. 4 The true stress–strain response for TC4 alloy at different strain rates.

tested with the tensile axis parallel to the normal direction in the plate, and fails along a shear plane that is oriented at 45° to the axis of loading.

2.3. Identified model constants

The true stress–strain response of the specimens is considerably more uniform and can be taken as the average curve through the valid data in Fig. 4. It shows that the TC4 alloy represents significant strain rate effect and the dynamic yield stress enhances significantly with the strain rate increasing. Failure in the specimens is supposed to occur at the point of pronounced necking or brittle fracture. The failure strain ε_f is calculated from the zone reduction in terms of the diameter of the fracture cross-section d_f and the initial diameter of the gauge section of the round bar d_0[12]:

$$\varepsilon_f = 2\ln(d_0/d_f) \tag{2}$$

The mean failure strains ε_f for the TC4 alloy tested in quasi-static and dynamic tensile tests at different strain rates are presented in Table 1. It can be seen that the fluctuation of the failure strains among the different strain rate tests obtained from material tests is not obvious. These values imply constant failure criterion is feasible for describing the failure of TC4 alloy. In practice, determining the failure strain requires consideration of several factors such as the failure mode (shear localization), the influence of strain rate and temperature,[13,14] as well as the mesh size of the finite element model,[15,16] which should be consistent with the results of ballistic impact tests.

The strain rate parameters C and p for TC4 alloy are determined by fitting yield stress at different strain rates using the least-squares method. The plastic hardening modulus E_p is given by the following equation:

$$E_p = \frac{E_t E}{E - E_t} \tag{3}$$

where E_t is the tangent modulus which is obtained by taking the slope of the plastic deformation part of the quasi-static stress–strain curves, E the elastic modulus. The harden law of TC4 alloy should take into account the Bauschinger effect.[17] While in continuum mechanics, this effect is regarded as a nonlinear isotropic/kinematic (mixed) hardening material feature in a constitutive model, so β takes a value of 0.21. The identification of constitutive parameters for the P-K constitutive model is listed in Table 2. The constitutive parameters of projectile material TA11 is given by China Standard Press.[18] It is assumed that the projectile deformation is independent on the strain rate effect in the range of impact velocities in the test; therefore, zero is defined as the strain rate parameter C and p values.

2.4. Finite element model

In the finite element model, the flat casing (FC) model is constrained on two sides, while the subscale casing (SC) model is constrained on three sides, which simulate the boundary condition of two series simulation casings of ballistic tests. Each case is performed using hexahedron mesh with reduced integrated element being used to avoid the excessive element distortion and error termination of the program. A total of 80400 elements are applied in two models. In order to capture the failure of global dishing and localized ductile tearing in the target, 4 elements through the thickness are used, besides, the element edge length of 1 mm in x and y directions is made in the impact zone and the elements in the periphery of the target are quite coarser. The finite element model is presented in Fig. 5. In explicit finite element analysis, a constant of 0.16 failure strain for TC4 alloy is set to reflect the ballistic impact results which are appropriate for the particular mesh sizes. To simulate perforation of the target, the element-kill algorithm is applied in LS-DYNA that eliminates the damaged elements from the mesh after the plastic strain exceeds the failure strain. Those elements no longer contribute to the overall response determination.

Table 1 Failure strain for TC4 alloy by material test.

Strain rate (s^{-1})	0.001	0.01	500	1000	2000	4000
Yield stress σ (MPa)	919	950	1135	1177	1219	1314
Failure strain ε_f	0.316	0.316	>0.045	>0.151	0.306	0.301

Table 2 Parameters for P-K model.

Material	E (GPa)	σ_0 (MPa)	μ	ρ (kg/m^3)	C ($10^5 s^{-1}$)	p	β	E_p (MPa)
TC4	109	919	0.34	4440	1.53	4.73	0.21	976.4
TA11	124	985	0.30	4370	0	0	0	0

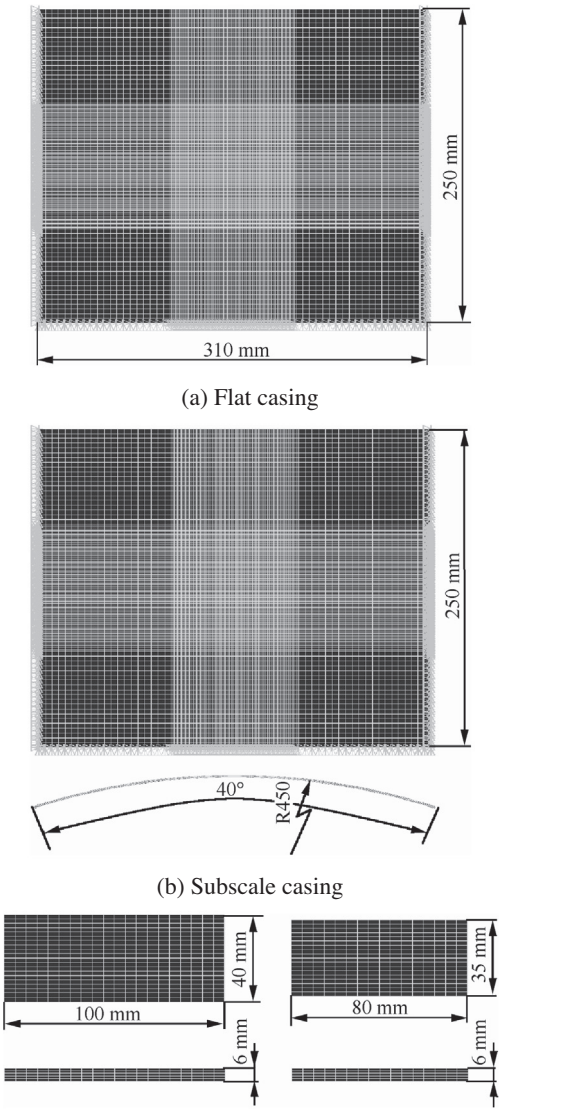

(a) Flat casing

(b) Subscale casing

(c) Large and small projectiles

Fig. 5 Finite element model of flat and subscale casings upon the projectile impact.

The eroding surface-to-surface contact algorithm is chosen to describe the interface interaction between projectile and target material in the simulation of penetration. It insures that after the failure elements are removed, the contact algorithm is still considered in other elements. The effect of friction is modeled by adjusting the static and dynamic coefficient of friction which is assumed to be 0.15 and 0.05 to imitate the process of the target perforation. The damping is used to diminish over time and eventually stop the vibrations caused by the energy dissipation mechanism.[19] However, the damping is not easy to determine in complex problems, so the recommended mass damping coefficient in LS-DYNA is set to $0.4\pi/T$, where T is period of fundamental mode of the target. To control the hourglassing effect which is possibly caused by the reduced integrated element, the viscosity-based hourglass control is opened for the target and projectile parts.

3. Numerical simulation of two series tests

In the simulation, the projectile is given an initial velocity identical and orientated to the one used in a corresponding test and the residual velocity of the projectile is registered. Details of each test simulation conditions, residual velocity, and absorbed energy are shown in Table 3. In comparison between the penetrated cases of FC tests, it seems that the critical velocities of subscale and flat casings are somewhat overestimated by the simulation. It should be explained that the residual velocities of the penetration cases are not exactly 0, because, in those cases of penetration, after impacting the target, projectile whirls and does not follow the x-axis direction. However, based on analyzing the pictures obtained by a high speed camera, the residual velocity in this occasion is very low.

The localized fracture appearances and plastic strain contour in the impact zone are illustrated in Fig. 6 by simulating two series of tests. It is shown that damage modes in both flat and subscale casings are very similar and all fracture characteristics are coincided with the corresponding test.[1] The failure mechanisms of flat and subscale casings are revealed from two typical case instances. The similarities of two kinds of targets are shown in Fig. 7. At initial contact of the projectile, the target mass in a highly localized zone is accelerated by the projectile immediately and the plastic wave propagates to the rear surface of the target. As the plastic strain of the target in the contact zone reaches to the failure strain, a crack is initiated by eroding the damaged elements, and then it is rapidly propagated in the rear surface of the target in the impact zone. At this moment, if the impact load is greater than the elastic restoring force and the friction caused by interactive scrap, this leads to the perforation of the target in the end, while if the impact load is less, it brings out penetration of the target. The damage of targets is also observed by simulating the two types of casings. These are in agreement with those of the test, including the global tensile failure and localized shear.

3.1. Energy analysis

Energy absorption is a major measurement index to evaluate the casing containment capability. For a hardwall fan casing, higher penetration resistance signifies more energy absorption. It shows that the capability of energy absorption of the targets in the numerical simulation is underestimated. The relative error between the test and the simulation is used to weigh the difference in absorbed energy. Compared to the test, the absorbed energy estimated by the numerical simulation is inclined to conservative. The main reason is that the energy of interactive scrap between the target and the projectile may be underestimated. The maximum deviation of the absorbed energy between the test and the simulation is 12.2%, which is acceptable concerning the complexity of the problem as ballistic impact.

During the impact, kinetic energy of the projectile is transferred to the target and absorbed through various energy consumption mechanisms, thereby increasing deformation energy of the system. The time variations of energy for the projectile and the target of FC5 and SC5 tests are shown in Fig. 8. The energy dissipation from the projectile is less than 1/10 of that from the target. This provides an indication that most energy is consumed by target deformation and fracture. Based on

Table 3 Comparison of test and numerical simulation.

Test No.	Thickness (mm)	Projectile mass (kg)	Obliquity (°)	Projectile orientation (°)			Initial velocity (m/s)
				Roll	Pitch	Yaw	
FC1	2.0	0.105	0	−25	−2	3	145.4
FC2	2.0	0.105	0	−15	−5	−6	76.1
FC3	2.0	0.105	15	−10	0	−2	74.8
FC4	2.0	0.073	0	−27	3	15	75.7
FC5	1.5	0.105	0	0	0	−10	66.2
FC6	2.5	0.105	0	−3	2	−1	74.2
SC1	2.0	0.105	0	0	0	12	126.5
SC2	2.0	0.105	0	−2	2	3	65.1
SC3	2.0	0.105	15	−20	−2	3	75.8
SC4	2.0	0.073	0	−10	5	−3	63.7
SC5	1.5	0.105	0	0	0	15	69.4
SC6	2.5	0.105	0	10	0	0	70.1

Test No.	Residual velocity (m/s)		Test result	Absorption energy (J)		
	Test	Numerical		Test	Numerical	Error (%)
FC1	—	105.8	Perforation	—	522.2	—
FC2	0	−23.2	Penetration	304.0	275.8	9.3
FC3	0	−22.8	Penetration	293.7	266.4	9.3
FC4	—	−9.8	Rebound	—	205.7	—
FC5	0	2.0	Perforation	230.1	229.9	0.1
FC6	−8.0	−20.8	Rebound	285.7	266.3	6.8
SC1	—	65.8	Perforation	—	612.8	—
SC2	—	−14.9	Rebound	—	210.8	—
SC3	0	26.4	Perforation	301.6	265.1	12.1
SC4	—	−24.5	Rebound	—	126.2	—
SC5	0	−6.1	Penetration	252.9	250.9	0.8
SC6	−17.1	−29.3	Rebound	242.6	212.9	12.2

Fig. 8(a) and (b), the common ground with respect to energy variations is reached. The energy curves of the projectile and the target could be divided into three stages. The first stage (Stage I) is that kinetic energy of the projectile has a nearly linear decrease with deformation energy of the system accumulated, which is called compression stage. The drop of kinetic energy is observed in the following stage (Stage II) which is entitled damage fracture stage from crack initiation till fracture of the target. In this stage, part of kinetic energy is transferred to internal energy. Then the kinetic energy curve of the projectile tends to be mild. The third stage (Stage III) which is characterized by the conversion from kinetic energy to deformation energy of the system due to damping and interactive scrap is called interactive scrap stage. It is reflected that main energy of the projectile is consumed by the elastic deformation and rupture of the target as Stages I and II show.

There are several minor exceptions which should be noted. In the numerical analysis, the global dishing of targets does not take on. This may cause a problem that it takes a long time for the attenuation of vibration energy of the targets, which requires a long time to run the nonlinear finite element analysis. In addition, the friction between the projectile and the target during perforation is mutative, that is because of the contact area and pressure. Therefore, a constant coefficient of friction is not enough to explain the real situation as observed in the ballistic test. Such changes might influence the global dishing, but the accurate friction coefficient between the casing and the projectile over the range of velocities in the test cannot be ac-

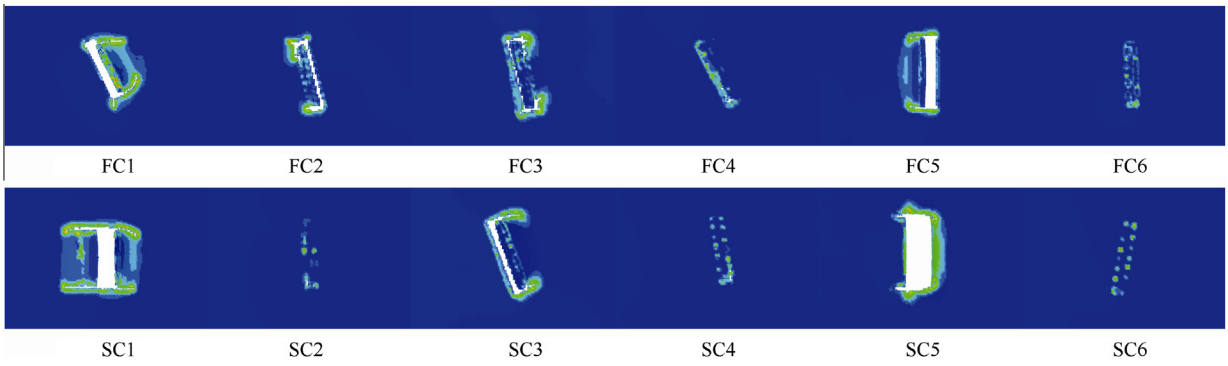

Fig. 6 Fracture appearances and plastic strain contour of the flat and subscale casing front surfaces.

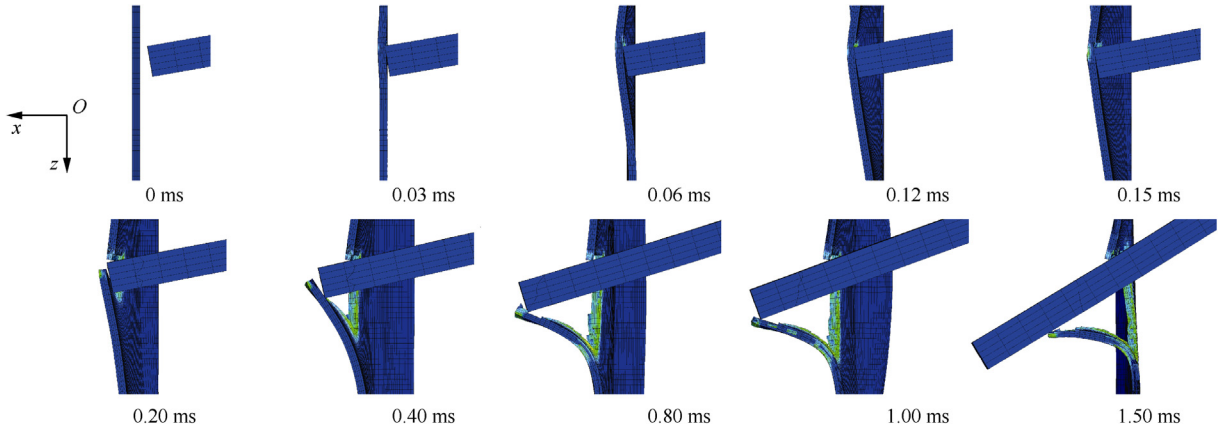

(a) Perforation of a 1.5 mm thick flat casing simulated on test FC5

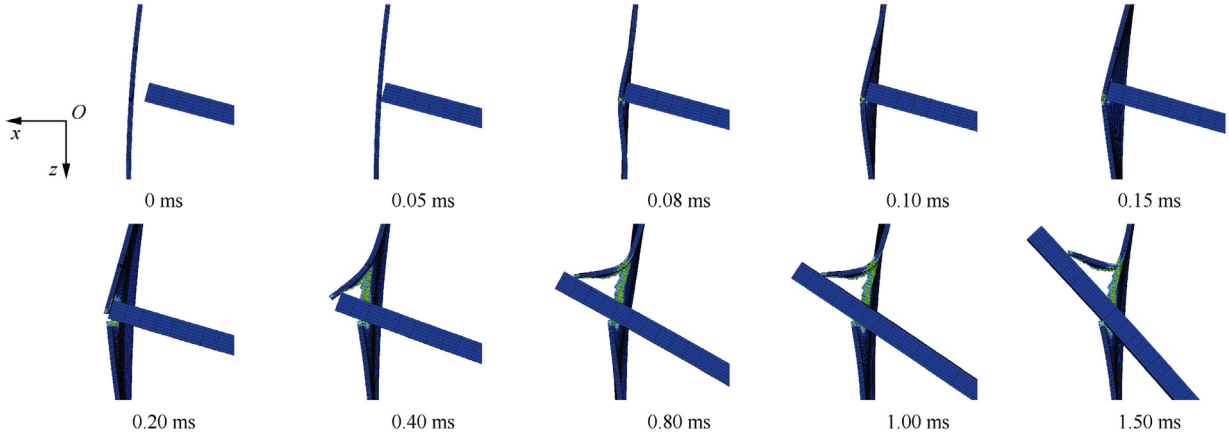

(b) Perforation of a 1.5 mm thick subscale casing simulated on test SC5

Fig. 7 Sectional view of the target perforation process for cuboids projectile.

quired easily.[20] However, those deficiencies do not significantly affect the energy estimated in the impact.

3.2. Analysis of critical velocity

Critical velocity of the projectile is another measurement index of containment capability of the target. However, based on the stochastic impact orientation and the different launch velocities in limited tests, there are some difficulties in direct determination of the critical velocity. According to practical experience, comprehensive consideration of above factors as an effect indicator is defined as follows:

$$\text{Effect indicator} = \frac{t_T}{S_T m_P^{1/2}} \tag{4}$$

where t_T is the target thickness, S_T the projected zone area, and m_P the mass of the projectile. The projected zone is the zone on the target along the launch direction. For a cuboids projectile, the projected zone is changed drastically with the three Tait-Bryan angles as defined in the first part of this paper. Compared with the projectile, curvature of the subscale casing is quite smaller. Therefore, it is simplified that the flat casing is substituted for the subscale casing to calculate the projected zone in the analysis.

Fig. 9 shows the influence of the target thickness, the projectile mass and projection zone on the critical velocity of two kinds of casings. It is denoted that the relationship between the comprehensive impact factor and the critical velocity is essentially linear over the velocity range of the impact test. The curve obtained is combined with the numerical simulation results by calculating the arithmetic average of the lowest perforation velocity and the highest rebounded velocity. The open symbols in the Fig. 9 are obtained from simulation by adding half of the lowest perforation velocity and half of the highest rebounded velocity, while the closed symbols are based on the ballistic tests. The dashed line connects the rebound and perforation test data and their homologous critical velocity is estimated by simulation.

It should be pointed out that the linear relationship between effect indicator and critical velocity presented in Fig. 9 should be suitable for a specific range. Subjected to a certain launch conditions, the variation of the target's thickness changes the failure mode from petaling, mixed plug/petal, to plugging,[21] while the critical velocity is no longer the linear variation. In addition, the projected zone is associated with the pitch and yaw angle, which are more sensitive to the critical velocity.[22] However, the linear relationship between impact angle and critical velocity maintains in an inter-cell, and the excessive angle

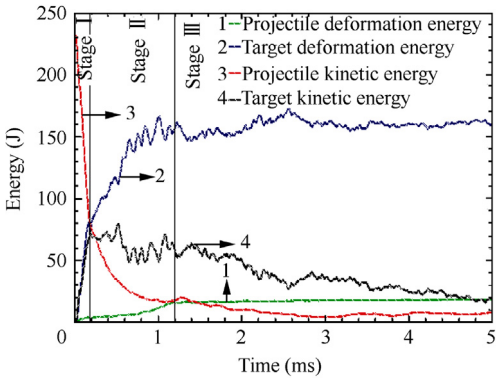

(a) Time variations of energy for FC5 test

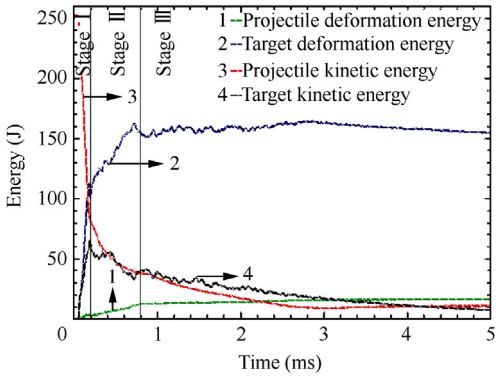

(b) Time variations of energy for SC5 test

Fig. 8 Three stages of energy variation.

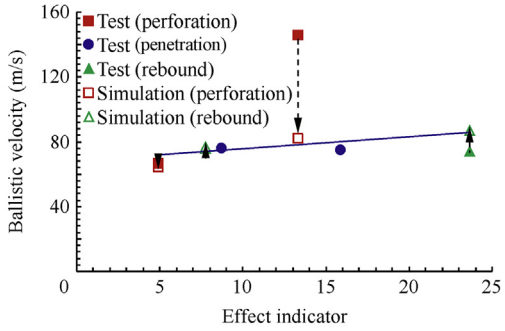

(a) Critical velocity of the flat casing

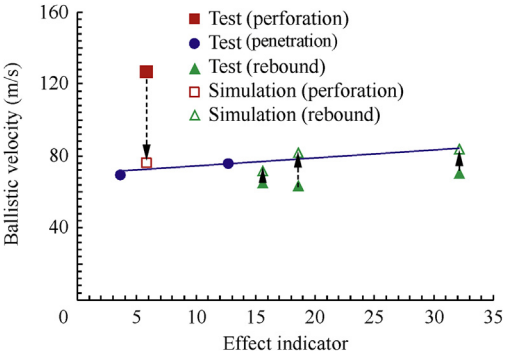

(b) Critical velocity of the subscale casing

Fig. 9 Effect of comprehensive impact factor on critical velocity of target.

may lead to complicated secondary impact. Individual factor's effect on critical velocity from a wide range is difficult to bring to light, which should consult a large number of test data.

4. Discussion

The effect indicator is introduced to discuss the penetration resistance of flat and subscale casings. Figure 10 is a drawing of the critical velocity of flat and subscale casings changing with the effect indicator which is determined by combining the test and numerical simulation. The data of flat and subscale casings appears to have significant scatter on a linear regression fit. As the friction between the target and the projectile is essential to the critical velocity in the actual test, the critical velocity is not unique. Therefore, probabilistic regions of the critical velocity of two types of casings are defined, supposing that the boundaries of the regions are parallel to the regression line and go through the maximum deviation of data.

With comparison of regional distribution of critical velocity between flat and subscale casings, some conclusions can be quickly drawn. Two tendencies exist: at one of very large impact angles with heavy projectile impact, the penetration resistance of the subscale casing is superior to the flat casing; at another angle close to the impact with lighter projectile impact, a converse conclusion is revealed. It seems that at a small-angle impact, the localized strength of the target material may be effective to penetration resistance, consequently enhancing the containment capability. Meanwhile, at a large-angle impact, besides the localized strength, the structure stiffness also plays an important role in the containment capability. However, in the real events of fan blade out, the failed blade moves towards the casing in a tangential path due to the rotational speed of the rotor, and after the first impact, the blade curls into a "U" shape.[23,24] So the impact of failed blade to the casing follows large angles, which is in accordance with the latter conclusion. That means the critical velocity obtained by the flat casing should be underestimated in the real containment of the failed blade.

5. Conclusions

(1) According to analysis of the energy of the system, the consumption mechanisms reveal that most energy is dissipative in the way of target deformation and fracture.

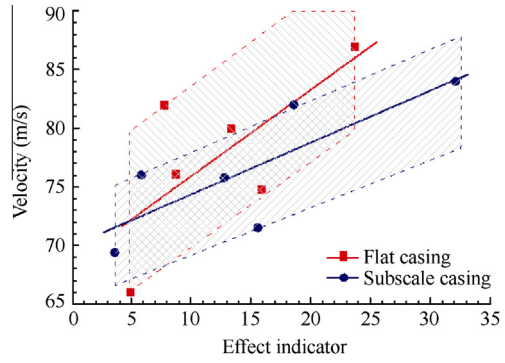

Fig. 10 Critical velocity of flat and subscale casings.

Considering the changing in the energy curve, it is summed up as compression stage, energy conversion stage, and interactive scrap stage.

(2) The linear variation of the critical velocity is identified with variation of the effect indicator which involves all the possible factors in the tests. Comprehensive analysis of the regional distribution of critical velocity reveals that the critical velocity obtained by the flat casing should be underestimated in the real containment of the failed blade.

6. Recommendations

This paper has provided an effective numerical simulation technology to clarify the penetration resistance of TC4 alloy. Two important evaluation indices of containment capability are used to research the impact response of the target material. However, the results are not expected to be adapted to all impact situations and some simulation parameters such as structure damping and friction coefficient during the punching need further research.

Future work should emphasize a great number of ballistic tests over a wider range of impact situations, and statistical analysis could be used to analyze the influence of impact angle.

Acknowledgements

The authors wish to thank Prof. Zang Chaoping of Nanjing University of Aeronautics and Astronautics for his support and valuable suggestions. Thanks are also given to Mr. Zhang Kewei, Mr. Liu Xuyang, Mr. Yang Le, and Miss Shi Qizhen for their help with experiments. Finally, the authors would like to thank the reviewers who provided very positive feedback that has resulted in a technically improved paper.

References

1. Zhang T, Chen W, Guan YP, Gao DP. Study on titanium alloy TC4 ballistic penetration resistance part I: ballistic impact tests. *Chin J Aeronaut* 2012;**25**(3):388–95.
2. Shmotin YN, Gabov DV, Ryabov AA, Kukanov SS, Rechkin VN. Numerical analysis of aircraft engine fan blade-out. In: *42nd AIAA/ASME/SAE/ASEE joint propulsion conference*; 2006. p. 2066–4620.
3. Sinha SK, Dorbala S. Dynamic loads in the fan containment structure of a turbofan engine. *J Aerosp Eng* 2009;**22**(3):260–9.
4. Belytschko T. On difficulty levels in non linear finite element analysis of solids. In: *Fourth IACM world congress on computational mechanics*; 1996. p. 6–8.
5. Jonas GH, Zukas JA. Mechanics of penetration: analysis and experiment. *Int J Eng.Sci* 1978;**16**(11):879–903.
6. Zhao X, Li Q. Dynamic properties of TC-4 titanium under high strain-rate. *Explosion Shock Waves* 1990;**10**(3):239–43 [Chinese].
7. Boyer R, Collings EW, Welsch G. *Materials properties handbook: titanium alloys*. 4th ed. Novelty, OH: ASM International; 1994.
8. Kurtaran H, Buyuk M, Eskandarian A. Ballistic impact simulation of GT model vehicle door using finite element method. *Theoret Appl Fract Mech* 2003;**40**(2):113–21.
9. Sharma AC, Sewak B, Singh M. Simulation of impact and penetration with hydrocodes. In: *SpringSim '08 proceedings of the 2008 spring simulation multiconference*; 2008. p. 729–36.
10. Jones N. Structural aspects of ship collisions. In: Jones N, editor. *Structural crashworthiness*. London: Butterworth and Company Publishers Limited; 1983. p. 308–37.
11. Happquist JO. *LS-DYNA theory manual*. Livermore, CA: Livermore Software Technology Corporation; 2005.
12. Teng X, Wierzbicki T. Evaluation of six fracture models in high velocity perforation. *Eng Fract Mech* 2006;**73**(12):1653–78.
13. Kay G. *Failure modeling of titanium 6Al–4V and aluminum 2024–T3 with the Johnson-Cook material model*; 2003. Report No.: DOT/FAA/AR-03/57.
14. Lesuer DR. *Experimental investigations of material models for Ti–6A1–4V titanium and 2024–T3 aluminum*; 2000. Report No.: DOT/FAA/AR-00/25.
15. Carney KS, Pereira JM, Revilock DM, Matheny P. Jet engine fan blade containment using an alternate geometry. *Int J Impact Eng* 2009;**36**(5):720–8.
16. Buyuk M, Kan S, Loikkanen MJ. Explicit finite-element analysis of 2024–T3/T351 aluminum material under impact loading for airplane engine containment and fragment shielding. *J Aerosp Eng* 2009;**22**(3):287–95.
17. Boyce BL, Chen X, Peters JO, Hutchinson JW, Ritchie RO. Mechanical relaxation of localized residual stresses associated with foreign object damage. *Mater Sci Eng A* 2003;**349**(1):48–58.
18. Ma J, Li C, Deng J. *Materials properties handbook: titanium alloys*. 2nd ed. Beijing: China Standard Press; 1994 [Chinese].
19. John OH. *LS-DYNA keyword user's manual*. 4th ed. Livermore, CA: Livermore Software Technology Corporation; 2006.
20. Yabuki A, Matsuwaki K, Matsumura M. Critical impact velocity in the solid particles impact erosion of metallic materials. *Wear* 1999;**233–235**:468–75.
21. Gogolewski RP, Cunningham BJ. *Terminal ballistic experiments for the development of turbine engine blade containment technology*; 1995. Report No.: UCRL-ID-120930.
22. Ambur DR, Jaunky N, Lawson RE, Knight NF, Lyle KH. A gas-actuated projectile launcher for high-energy impact testing of structures. In: *40th structures, structures dynamics, and materials conference*; 1999. p. 1–11.
23. Xuan HJ, Wu RR. Aeroengine turbine blade containment tests using high-speed rotor spin testing facility. *Aerosp Sci Technol* 2006;**10**(6):501–8.
24. Heermann KF. *Study to improve turbine engine rotor blade containment*; 1977. Report No.: FAA-RD-77-44.

Zhang Tao is a Ph.D. candidate at Nanjing University of Aeronautics and Astronautics. His main research interests are aeroengine safety assessment of blade containment and technology of airworthiness compliance verification.

Chen Wei is a professor at Nanjing University of Aeronautics and Astronautics (NUAA). He received his B.S. and Ph.D. degrees from NUAA in 1990 and 1995, respectively. His research interests are structure, strength, vibration, and reliability of aeroengines.

Guan Yupu is a professor at Nanjing University of Aeronautics and Astronautics. He received his B.S. and M.S. degrees from Jilin University of Technology in 1982 and 1986, respectively. In 1992 he received his Ph.D. degree from Dalian University of Technology. His research interests are computational structural mechanics and structure, strength, and vibration of aeroengines.

Gao Deping is a professor at Nanjing University of Aeronautics and Astronautics. He has a lofty fame in structure, strength, and vibration of aeroengines.

Li Shuguang is a manager in the Engineering Department at CITIC Offshore Helicopter Co., Ltd. He received B.S. degree from Nanjing University of Aeronautics and Astronautics in 1993. His research interests include structure and strength of aeroengines.